Vol. 92 No. 2 pp. 876–878 ACTA GEOLOGICA SINICA (English Edition) Apr. 2018

Research Advances

Zircon U-Pb Dating of Leucogranite in Lhozag and Its Geological Significance

GUO Linnan[1], HUANG Chunmei[1, 2, *], SHI Qingshang[2] and YAN Jingjing[2]

1 *Chengdu Center, China Geological Survey, Chengdu 610081, China*
2 *School of Geosciences and Resources, China University of Geosciences, Beijing 100083, China*

Objective

The Himalayan leucograite, which is typical production of continent-continent collision orogenic belt, has become a research hotspot of the Tibetan Plateau. The research on the leucogranite would help to verify and improve the continent-continent collision orogenic theory. (Huang et al., 2017; Fig. 1a). Previous studies show the Himalayan leucogranite was mainly melted from crust materials (Guo and Wilson, 2012). But it remains controversial for the formation model as to whether it formed from gathering of dikes or diaper of deep magma chambers. The Himalayan leucogranite can be divided into Tethyan Himalayan leucogranite in the north and High Himalayan leucogranite in the south by the Southern Tibetan Detachment System (STDS) (Yin et al., 2006; Fig. 1b). The Lhozhag area, located in the eastern part of the High Himalayan leucogranite belt and develops a large amount of tourmaline leucogranite, garnet leucogranite and two-mica granite, is an ideal area to verify their formation model. This study firstly tries to probe the formation process of the Lhozag leucogranites with the zircon U-Pb dating.

Methods

This study performs U-Pb isotopic dating on a garnet leucogranite sample from Lhozag. zircons were separated by heavy-liquid and magnetic methods. The internal growth structure of zircon grains was revealed with the cathodoluminescence (CL) imaging technique at the Institute of Geology and Geophysics, Chinese Academy of Sciences. One part of the zircon U-Pb dating spots was done using LA-ICP-MS at the Key Laboratory of Metallogeny and Mineral Assessment, Institute of Mineral Resources, CAGS. Laser sampling was performed using a Newwave UP 213 laser ablation system. A Thermo Finnigan Neptune MC-ICP-MS instrument was used to acquire ion-signal intensities. Off-line raw data selection and integration of background and analyze signals, and time-drift correction and quantitative calibration for U-Pb dating was performed with the by ICPMSDataCal. The other part of the zircon U-Pb dating spots was performed using LA-ICP-MS at the Key Laboratory of Orogenic Belts and Crustal Evolution, Peking University. Isotopic ratios of zircons were calculated using GLITTER (ver. 4.4). Concordia ages and diagrams were obtained using Isoplot/Ex (3.0). The common lead was corrected using LA-ICP-MS Common Lead Correction, followed the method of Andersen (2002).

* Corresponding author. E-mail: huangchunmei0126@163.com

Result

The CL images show that the zircon grains are euhedral -subhedral with long columnar shape, and range in a size from 90 to 150 μm with aspect ratios of 1:1–1:3. The zircon grains normally show spongy texture in the core due to the dissolution by fluids. And the rims normally show oscillatory zonings. The CL images generally show weak luminescence because of high contents of radioactive elements. This study performs 40 spots analyses with 34 efficient spots. The old zircons with strong luminescence contain U of 142–1818 ppm, Th of 96–1136 ppm, with Th/U rations of 0.2–1.3. Their $^{206}Pb/^{238}U$ ages range from 411 to 784 Ma. The rims which exhibit clear oscillatory zoning with weak luminescence contain higher U of 694–9537 ppm, Th lower than 286 ppm, with Th/U ratios lower than 0.1, indicating that they crystallized from the anatectic melt. The $^{206}Pb/^{238}U$ ages range from 17.1 Ma to 28.5 Ma, with two clusters of 24.1±0.5 Ma (MSWD=3.3, n=7) and 17.7±0.4 Ma (MSWD = 2.1, n=9) (Fig. 1c).

Conclusion

The granitic rocks alternatively form from assembling of dikes or diapirism of magma chambers. The maximum time span for granitoid formed from diapirism of magma chambers can't be more than 1 Ma. The age spectrum

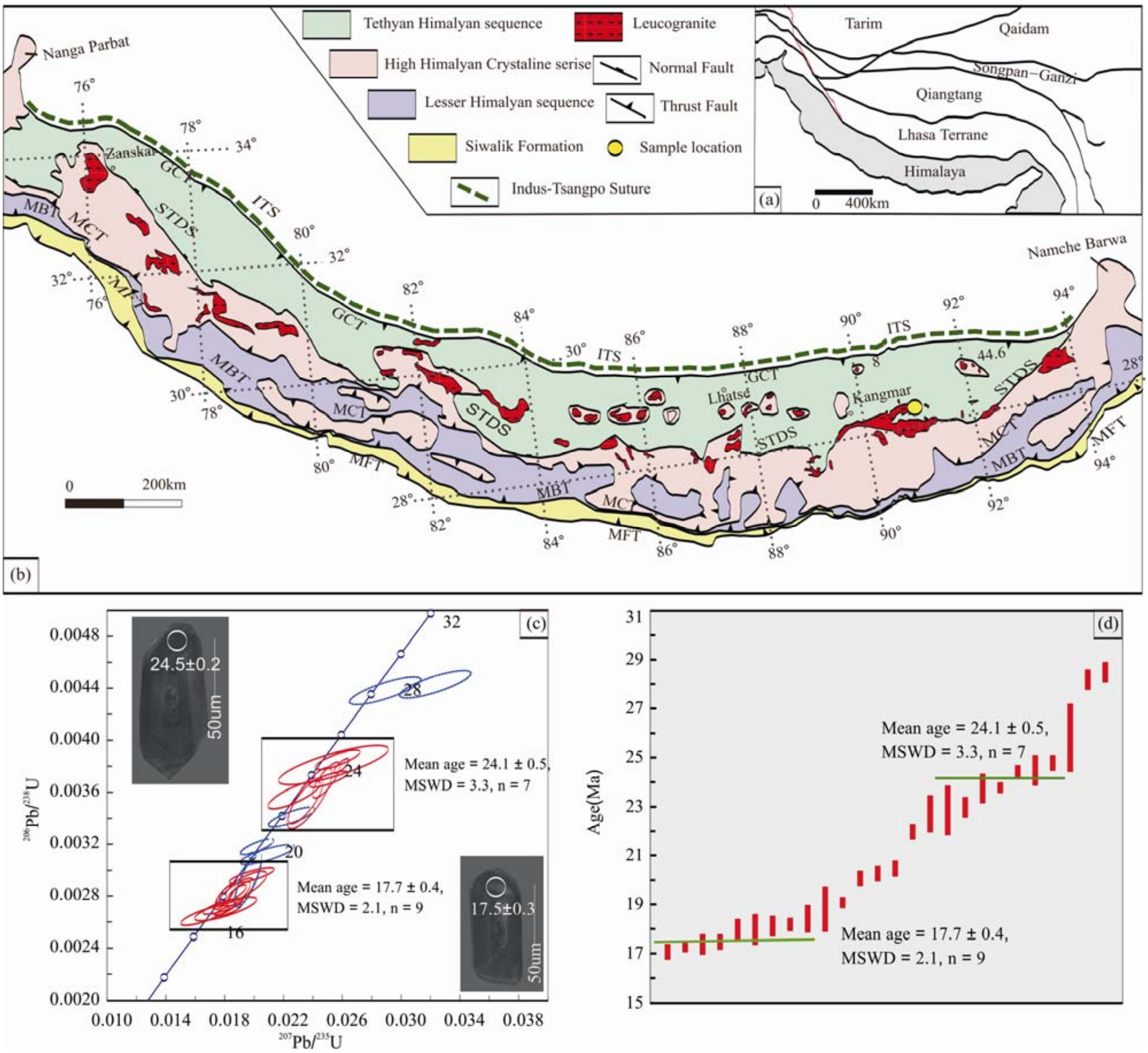

Fig. 1. (a) Simplified map of tectonic boundaries and units of Himalaya; (b) simplified geologic map of the Himalayan orogenic belt; (c) the zircon U-Pb dating concordia diagram and (d) age spectrum diagram of the Lhozag leucogranite.

diagram of the leucogranite shows the anatexis of Lhozag area started from 28.5 Ma and continued to 17.1 Ma with two intense melting events respectively at 24.1 Ma and 17.7 Ma (Fig. 1d), which is much longer than the time span of diapirism of magma chambers. All of these zircon U-Pb age results are continuous increasing and that results are with minor errors individually (Fig. 1d), which illustrate that the Lhozag leucogranite was derived from protracted melting of crust.. Therefore, the leucogranite in Lhozag is considered to be assembled by diking.

Acknowledgments

This research was supported by the National Key Research and Development Project of China (project 2016YFC0600304), the National Key Project on Basic Research of China (project 2015CB452604), and the Strategic Priority Re-search Program (B) of the Chinese Academy of Sciences (project XDB03010301).

References

Guo, Z.F., and Wilson, M., 2012. The Himalayan leucogranites: constraints on the nature of their crustal source region and geodynamic setting. *Gondwana Res.*, 2012, 22(2): 360–376.

Huang, C.M., Zhao, Z.D., Li, G.M., Zhu, D.C., Liu, D., and Shi, Q.S., 2017. Leucogranites in Lhozag, southern Tibet: Implications for the tectonic evolution of the eastern Himalaya. *Lithos*, 294: 246–262.

Yin, A., 2006. Cenozoic tectonic evolution of the Himalayan orogen as constrained by along-strike variation of structural geometry, exhumation history, and foreland sedimentation. *Earth-Sci. Rev.*, 76(1-2): 1–131.

Appendix 1 The zircon U-Pb isotopic data of the Lhozag leucogranite

Spot No.	Content (ppm)			Th/U	Isotope ratio						Age (Ma)					
	Pb	Th	U		$^{207}Pb/^{206}Pb$	1σ	$^{207}Pb/^{235}U$	1σ	$^{206}Pb/^{238}U$	1σ	$^{207}Pb/^{206}Pb$	1σ	$^{207}Pb/^{235}U$	1σ	$^{206}Pb/^{238}U$	1σ
LZH1121-1	144	126	168	0.75	0.05867	0.00057	0.60668	0.00627	0.07501	0.00028	553.7	-12.0	481.5	4.0	466.2	1.7
LZH1121-2	42	56	1836	0.03	0.07496	0.00124	0.03838	0.00074	0.00371	0.00004	1133.3	33.3	38.2	0.7	23.9	0.3
LZH1121-3	24	5	731	0.01	0.06139	0.00173	0.03098	0.00102	0.00366	0.00003	653.7	65.7	31.0	1.0	23.5	0.2
LZH1121-4	202	157	964	0.16	0.05753	0.00040	0.15502	0.00159	0.01954	0.00014	522.3	14.8	146.3	1.4	124.8	0.9
LZH1121-5	211	96	418	0.23	0.06125	0.00063	0.61058	0.00668	0.07232	0.00038	647.9	50.0	483.9	4.2	450.1	2.3
LZH1121-6	445	223	209	1.07	0.07150	0.00052	1.15977	0.03588	0.11763	0.00336	972.2	10.2	781.8	16.9	716.9	19.4
LZH1121-7	28	93	3195	0.03	0.04951	0.00050	0.02594	0.00034	0.00380	0.00004	172.3	24.1	26.0	0.3	24.5	0.2
LZH1121-8	18	20	568	0.04	0.08133	0.00179	0.04846	0.00124	0.00432	0.00004	1229.3	42.6	48.0	1.2	27.8	0.3
LZH1121-9	8	1	1312	0.00	0.04850	0.00244	0.01859	0.00092	0.00280	0.00009	124.2	-80.5	18.7	0.9	18.0	0.6
LZH1121-10	2	0	1382	0.00	0.04831	0.00088	0.01884	0.00042	0.00283	0.00004	122.3	44.4	18.9	0.4	18.2	0.2
LZH1121-11	38	54	1792	0.03	0.05124	0.00113	0.02820	0.00096	0.00401	0.00021	250.1	45.4	28.2	0.9	25.8	1.4
LZH1121-12	5	74	1769	0.04	0.04832	0.00065	0.02351	0.00078	0.00353	0.00011	122.3	31.5	23.6	0.8	22.7	0.7
LZH1121-13	23	0	1051	0.00	0.04880	0.00146	0.01960	0.00061	0.00293	0.00014	139.0	70.4	19.7	0.6	18.8	0.9
LZH1121-14	5	0	694	0.00	0.04836	0.00165	0.01916	0.00113	0.00287	0.00008	116.8	79.6	19.3	1.1	18.4	0.5
LZH1121-15	439	165	142	1.17	0.06909	0.00021	1.23131	0.01417	0.12934	0.00146	901.9	7.4	814.9	6.4	784.1	8.3
LZH1121-16	259	2796	32436	0.09	0.14243	0.00866	0.02407	0.00037	0.00155	0.00006	2257.1	105.3	24.2	0.4	10.0	0.4
LZH1121-17	22	130	2729	0.05	0.04894	0.00033	0.02491	0.00062	0.00369	0.00009	146.4	16.7	25.0	0.6	23.8	0.6
LZH1121-18	2	3	1021	0.00	0.04874	0.00071	0.01895	0.00052	0.00282	0.00006	200.1	33.3	19.1	0.5	18.1	0.4
LZH1121-19	2	1	1798	0.00	0.04670	0.00063	0.01800	0.00047	0.00280	0.00007	35.3	-167.6	18.1	0.5	18.0	0.4
LZH1121-20	3	46	1517	0.03	0.04860	0.00123	0.02377	0.00101	0.00355	0.00015	127.9	54.6	23.9	1.0	22.9	1.0
LZH1121-21	10	158	1536	0.10	0.02892	0.00160	0.00438	0.00007	0.01423	0.00046	95.0	94.0	29.0	2.0	28.2	0.4
LZH1121-22	8	13	1670	0.01	0.03233	0.00160	0.00443	0.00007	0.00242	0.00173	328.0	84.0	32.0	2.0	28.5	0.4
LZH1121-23	58	720	541	1.33	0.52047	0.01640	0.06748	0.00092	0.01964	0.00045	450.0	46.0	425.0	11.0	421.0	6.0
LZH1121-24	9	9	2023	0.00	0.02540	0.00247	0.00381	0.00010	0.01291	0.00495	116.0	167.0	25.0	2.0	24.5	0.6
LZH1121-25	254	56	1388	0.04	2.36204	0.03170	0.15013	0.00157	0.03455	0.00165	1866.0	11.0	1231.0	10.0	902.0	9.0
LZH1121-26	8	1	2770	0.00	0.01664	0.00108	0.00265	0.00005		0.01908		104.0	17.0	1.0	17.1	0.3
LZH1121-27	12	1	4023	0.00	0.01823	0.00060	0.00269	0.00003	0.01146	0.01352	158.0	56.0	18.3	0.6	17.3	0.2
LZH1121-28	33	186	7176	0.03	0.02508	0.00087	0.00370	0.00004	0.00117	0.00008	153.0	85.0	25.1	0.9	23.8	0.2
LZH1121-29	13	0	4092	0.00	0.01788	0.00090	0.00272	0.00004	0.03534	0.05131	85.0	85.0	18.0	0.9	17.5	0.3
LZH1121-30	26	140	6284	0.02	0.02255	0.00104	0.00341	0.00005	0.00108	0.00021	95.0	107.0	23.0	1.0	22.0	0.3
LZH1121-31	39	208	368	0.56	0.59239	0.02365	0.07554	0.00088	0.02348	0.00023	487.0	94.0	472.0	15.0	469.0	5.0
LZH1121-32	117	541	1173	0.46	0.59533	0.00930	0.07552	0.00078	0.02433	0.00046	499.0	17.0	474.0	6.0	469.0	5.0
LZH1121-33	37	286	9537	0.03	0.01984	0.00101	0.00296	0.00004	0.00094	0.00013	127.0	119.0	20.0	1.0	19.1	0.2
LZH1121-34	14	29	3368	0.01	0.02091	0.00122	0.00312	0.00005	0.00099	0.00068	130.0	137.0	21.0	1.0	20.1	0.3
LZH1121-35	162	1136	1818	0.62	0.51693	0.01057	0.06576	0.00074	0.01905	0.00042	493.0	26.0	423.0	7.0	411.0	4.0
LZH1121-36	14	29	2841	0.01	0.02273	0.00118	0.00358	0.00007	0.00404	0.00327		120.0	23.0	1.0	23.0	0.4
LZH1121-37	28	146	6323	0.02	0.02568	0.00101	0.00385	0.00005	0.00259	0.00032	119.0	67.0	25.7	1.0	24.8	0.3
LZH1121-38	41	253	9329	0.03	0.02021	0.00075	0.00318	0.00004	0.00160	0.00071		84.0	20.3	0.7	20.5	0.3
LZH1121-39	33	210	7498	0.03	0.02422	0.00169	0.00316	0.00005	0.00098	0.00013	438.0	164.0	24.0	2.0	20.3	0.3
LZH1121-40	7	1	2303	0.00	0.01807	0.00140	0.00270	0.00006	0.03578	0.02996	130.0	132.0	18.0	1.0	17.4	0.4